COMMUNICATIONS IN NUMERICAL METHODS IN ENGINEERING
Commun. Numer. Meth. Engng (2008)
Published online in Wiley InterScience (www.interscience.wiley.com). DOI: 10.1002/cnm.1157

Reconstruction-oriented multigrid finite element algorithm on bioluminescence tomography incorporating *priori* information

Jin Shi, Jie Tian*, †, ‡ and Min Xu

Medical Image Processing Group, Institute of Automation, Chinese Academy of Sciences, P.O. Box 2728, Beijing 100190, China

SUMMARY

Bioluminescence tomography (BLT) is employed to reconstruct internal bioluminescent source to reveal the molecular and cellular information. However, BLT faces many challenges such as quantitative reconstruction. In this paper, a reconstruction–oriented multigrid finite element algorithm is proposed to fully reconstruct the source density. A source permissible region is utilized to raise the numerical stability. The proposed algorithm transfers diffuse equation into liner relationship between the inner source and boundary information on a mesh. A tolerant algorithm for linearly constrained optimization algorithm can solve the box-constrained quadratic optimization problem. By setting a threshold as the average reconstruction densities, we can refine every possible source element and form next mesh until the reconstructed densities are accepted. Numerical simulation of homogeneous and heterogeneous phantom demonstrates the feasibility and potential of the proposed algorithm. Copyright © 2008 John Wiley & Sons, Ltd.

Received 27 March 2008; Revised 31 May 2008; Accepted 6 June 2008

KEY WORDS: bioluminescence tomography; reconstruction-oriented multigrid; *priori* information

*Correspondence to: Jie Tian, Medical Image Processing Group, Institute of Automation, Chinese Academy of Sciences, P.O. Box 2728, Beijing 100190, China.
†E-mail: tian@fingerpass.net.cn, tian@ieee.org
‡Senior member.

Contract/grant sponsor: National Key Basic Research and Development Program; contract/grant number: 2006CB705700
Contract/grant sponsor: Changjiang Scholars and Innovative Research Team in University (PCSIRT); contract/grant number: IRT0645
Contract/grant sponsor: CAS Hundred Talents Program, CAS Scientific Research Equipment Develop Program; contract/grant numbers: YZ0642, YZ200766
Contract/grant sponsor: 863 program; contract/grant number: 2006AA04Z216
Contract/grant sponsor: Joint Research Fund for Overseas Chinese Young Scholars; contract/grant number: 30528027
Contract/grant sponsor: National Natural Science Foundation of China; contract/grant numbers: 30672690, 30600151, 30500131, 60532050
Contract/grant sponsor: Beijing Natural Science Fund; contract/grant numbers: 4051002, 4071003

1. INTRODUCTION

Along with the advancement of genomics and proteomics, molecular imaging, especially small-animal molecular imaging acts an significant role that can bear comparison with traditional clinical imaging and microcosmic biological imaging [1]. Because of the high sensitivity, low cost and operation facility of the photonics-based imaging modalities, bioluminescence tomography (BLT) [2, 3], fluorescence molecular tomography (FMT) [4] and photoacoustic tomography (PAT) [5] are new imaging method *in vivo* that can dynamically and real-timely monitor the molecular and cellular activities, and hence report the growth and regression of tumor non-invasively. The principle of BLT and FMT is to retrieve light source information from the light flux detected on the surface of small animal. While FMT is a nonlinear inverse scattering problem, BLT belongs to the inverse source problem due to no demand of external light source and has a good signal-to-noise ratio (SNR). Before BLT experiment, the reporter genes are transfected into main organs of the small animal. At present, this injection method is used in the *in vivo* study of immune cell monitoring and various genetic controls [1]. In Bioluminescence tomography, luciferase enzymes are used to real-timely observe the tagged tumors in small animals. After it is injected into a living mouse, those cells in the aimed organism emit photons of light [6].

Bioluminescent photon propagation in biological tissue is governed by the radiative transfer equation (RTE) [3]. However, the RTE is expensive in computation in the practical small-animal environment. In contrast with absorption, scattering is the primary manner in the living animal, hence the diffusion equation is a relatively accurate approximation and has been widely adopted to describe photon propagation when the biological tissue has characteristic of high scattering optical property [7]. Based on diffusion approximation, the uniqueness theorem asserts that BLT reconstruction result is not unique [2]. In view of the ill-poseded characteristic of BLT, we can get some solutions that can match the boundary measurements. The uniqueness research on BLT shows that *a priori* knowledge can attribute to source reconstruction, such as the anatomical information and the background optical properties. Up to now, most BLT groups in the world get the optical properties of the main anatomical tissues from the literature [6, 8, 9], which cannot be very accurate in practice because of the diversity of individuals. On the other hand, three-dimensional BLT reconstruction is a high ill-posed inverse problem and it is difficult to fully reconstruct the source density information [10].

In this paper, we set up a source permissible region to reduce the dimensions and complexity of reconstruction. To reconstruct BLT light sources density, we propose reconstruction-oriented multigrid finite element algorithm (ROMFE) to raise the reconstruction accuracy of source density. A tolerant algorithm for linearly constrained optimization algorithm can iteratively solve this kind of least-squares problem. Let a threshold be the average reconstruction density of the former mesh, we can refine every possible source element and generate the finer mesh until the iterative reconstruction process receives the desired results. To avoid the inverse crime [11], the forward solver cannot be relevant to the inverse one. Molecular optical simulation environment (MOSE) [12] is utilized to generate the forward data, which is researched and developed based on statistical modeling and can depict bioluminescent photon transport in the biological tissue. Several numerical simulations of sources reconstructions show the feasibility and merits of the proposed reconstruction algorithm. In addition, we validate the importance of accurate spatial distribution of optical properties.

DOI: 10.1002/cnm

2. ALGORITHMS

2.1. Diffusion approximation and boundary condition

The tissues of small animal are turbid media in which photons are highly scattered and absorbed. Transport equation is regarded as an accurate mathematical model for transportation of photons in the body of small animals [3]. However, the RTE is difficult to be solved and highly computational. In practical environment, the influence of photon scattering is more important than that of photon absorption, hence we can utilize diffusion approximation to simulate the light transportation. In BLT, the measured optical signal is assumed to be continuously emitted by internal bioluminescent sources, so the propagation of light can be described by the steady-state diffusion equation and Robin boundary condition [6, 8] as below:

$$-\nabla\cdot(D(\mathbf{x})\nabla\Phi(\mathbf{x}))+\mu_{\mathrm{a}}(\mathbf{x})\Phi(\mathbf{x})=S(\mathbf{x})\quad(\mathbf{x}\in\Omega) \tag{1a}$$

$$\Phi(\mathbf{x})+2A(\mathbf{x};n,n')D(\mathbf{x})(\mathbf{v}(\mathbf{x})\cdot\nabla\Phi(\mathbf{x}))=0\quad(\mathbf{x}\in\partial\Omega) \tag{1b}$$

where Ω and $\partial\Omega$ are the tissue region and boundary correspondingly; $\Phi(x)$ represents the photon flux density distribution; $S(x)$ denotes source energy density distribution; $D(x)=1/[3(\mu_{\mathrm{a}}(x)+(1-g)\mu_{\mathrm{s}}(x))]$ is the diffusion coefficient; $\mu_{\mathrm{a}}(x)$ is the absorption coefficient, while $\mu_{\mathrm{s}}(x)$ is the scattering coefficient; and g is anisotropic parameter; v is the unit outer normal to $\partial\Omega$ at location x; $A=(1+R)/(1-R)$, in which R depends on the refraction properties of the medium and can be approximated by $R\approx-1.4399n^{-2}+0.7099n^{-1}+0.6681+0.0636n$ [13].

In bioluminescent tomography, the outgoing flux density $Q(x)$ can be measured by a highly sensitive CCD camera:

$$Q(\mathbf{x})=-D(\mathbf{x})(\mathbf{v}\cdot\nabla\Phi(\mathbf{x}))=\frac{\Phi(\mathbf{x})}{2A(\mathbf{x};n,n')}\quad(\mathbf{x}\in\partial\Omega) \tag{2}$$

Thus, BLT problem is defined as: reconstructing three-dimensional image information $S(x)$ from boundary measurement $Q(x)$ on the surface by Equations (1)–(2).

2.2. Reconstruction-oriented multigrid finite element algorithm

On the basis of finite element method [14, 15], the below weak form of steady-state diffusion can be detailed as follows:

$$\int_{\Omega}(D(\mathbf{x})(\nabla\Phi(\mathbf{x}))\cdot(\nabla\Psi(\mathbf{x}))+\mu_{\mathrm{a}}(\mathbf{x})\Phi(\mathbf{x})\Psi(\mathbf{x}))\,\mathrm{d}V$$
$$+\int_{\partial\Omega}\frac{1}{2A(\mathbf{x};n,n')}\Phi(\mathbf{x})\Psi(\mathbf{x})\,\mathrm{d}A=\int_{\Omega}S(\mathbf{x})\Psi(\mathbf{x})\,\mathrm{d}V,\quad\forall\Psi(x)\in H^1(\Omega) \tag{3}$$

From coarseness to fineness, Let $\{V_1,\ldots,V_k,\ldots\}$ be tetrahedron mesh on the domain Ω. Taking mesh V_k as an example, the left integrals of (3) can be written as the matrix multiplication of M^k

DOI: 10.1002/cnm

and Φ^k, where Φ^k represents the vector of the photon flux density on the mesh V_k and M^k is a symmetric, positive-definite and sparse matrix.

The right integrals are treated as follows: take any tetrahedron I^k as example:

$$\int_{I^k} S(\mathbf{x})\Psi(\mathbf{x})\,\mathrm{d}V = [\Psi^k_{i_1}\ \ \Psi^k_{i_2}\ \ \Psi^k_{i_3}\ \ \Psi^k_{i_4}] * [W^k_{i_1}\ \ W^k_{i_2}\ \ W^k_{i_3}\ \ W^k_{i_4}]^T * S^k_i \tag{4}$$

where S^k_i represents the ith reconstruction element on V_k; $\Psi^k_{i_1}, \Psi^k_{i_2}, \Psi^k_{i_3}, \Psi^k_{i_4}$ are the nodal variables of the element I^k; $W^k_{i_1}, W^k_{i_2}, W^k_{i_3}, W^k_{i_4}$ are the basis function of the element I^k, which can describe the spatial distribution and shape of the tetrahedron and can raise the source densities in reconstruction process.

And then we can form the linear equation between the source energy densities and the photon flux densities on the whole mesh V_k

$$M^k \Phi^k = F^k S^k \tag{5}$$

By deleting internal photon flux variables and source variables in source impermissible region, we can build the linear relationship between the unknown inner source and the photon flux density on the boundary on mesh V_k

$$M^k_{\mathrm{mod}} \Phi^k_{\mathrm{bound}} = F^k_{\mathrm{mod}} S^k_{\mathrm{pr}} \tag{6}$$

Hence, BLT problem can be described as a box-constrained quadratic optimization problem.

$$\min_{S^{\mathrm{low}}_k \leqslant S^{\mathrm{pr}}_k \ll S^{\mathrm{up}}_k} \{\| M^k_{\mathrm{mod}} \Phi^k_{\mathrm{bound}} - F^k_{\mathrm{mod}} S^k_{\mathrm{pr}} \|_\wedge + \lambda \xi(S^k_{\mathrm{pr}})\} \tag{7}$$

where S^{low}_k and S^{up}_k are the low and up bounds of the source density; $\wedge$ is the weight matrix, $\|V\|_\wedge = V^{\mathrm{T}} \wedge V$; λ is the regularization parameter; ξ is the penalty function. A tolerant algorithm for linearly constrained optimization can iteratively solve (7) perfectly [16].

A threshold S^{thres}_k can be set as the average reconstruction densities on V_k. We divide every possible source element greater than S^{thres}_k into eight son-tetrahedra and close the triangulation [17] and form next mesh V_{k+1} until the iterative reconstruction process receives the desired results. By using reconstruction-oriented multigrid algorithm, we can fully reconstruct the source density and reduce the ill-posedness of BLT.

2.3. Incorporation of a priori information

In the complex biological tissues, bioluminescent source generates photons that are highly scattered and absorbed in the body, which results in the difficulty of source quantification. Hence, bioluminescent source reconstruction problem is severely ill-posed. The theoretical uniqueness proof [2] tells that we cannot get unique reconstruction source in BLT if we do not incorporate some practical *a priori* information.

In this paper, we make a practical assumption on the distribution of real source that is divided into a source permissible region and a source impermissible region to enhance the computational efficiency and reconstruction stability and alleviate the ill-posedness of BLT. In Equation (5), the vector S^k stands for the source distribution on the whole mesh V_k. On the assumption, we can divide S^k into two sub vectors: S^k_{pr} and S^k_{upr}, which describes the distribution in source permissible region and that in source impermissible region correspondingly. Obviously, S^k_{upr} is zero vector

DOI: 10.1002/cnm

on assumption. By deleting internal photon flux variables and source energy density on source impermissible region, accompanied by matrix transformation of M^k and F^k, we can formulate the linear equation between the unknown inner source information and the photon flux density information on the boundary, which is shown in Equation (6).

On the other hand, by virtue of the characteristic of high ill-posedness of BLT, it is very important to evaluate background optical parameters accurately, which is used as essential *a priori* information for accurate BLT reconstruction. Currently, most BLT research groups acquire the optical properties of the main anatomical organs from the references that cannot be accurate actually. In homogeneous phantom, we use the optical parameters of 50% errors to show the importance of accurate background optical parameters in reconstruction.

3. EXPERIMENTAL RESULTS

3.1. Homogeneous experiment

To evaluate the proposed algorithm, two numerical simulations are carried out. In the first simulation, we use a homogeneous phantom. In Figure 1, the bioluminescent source of radius 1 mm and total power 1 W is centered in the spherical lung tissue, whose radius ranges from 1 to 10 mm.

We contrast forward solutions of the proposed algorithm and analytic formula as shown in Figure 2. In BLT field, the analytic formula is first used by BLT lab in Virginia Polytechnic Institute and State University [18]. The absorption coefficient $\mu_a = 0.12\,\mathrm{mm}^{-1}$, the scattering coefficient $\mu_s = 20\,\mathrm{mm}^{-1}$, the anisotropy parameter $g = 0.9$. The forward solution of the proposed algorithm meets with analytic solution generally in Figure 2.

Table I compares the forward solutions of ROMFE and analytic formula and shows ROMFE errors Err: $\mathrm{Err} = |\varnothing_{\mathrm{ana}} - \varnothing_{\mathrm{romfe}}|/2$. From Table I, we can see $\mu_a = 0.12\,\mathrm{mm}^{-1}$, $\mu_s = 20\,\mathrm{mm}^{-1}$, $g = 0.9$ agree with analytic formula. The relevant errors are mostly under 10%.

We compare ROMFE reconstruction with accurate optical coefficients to that with inaccurate coefficients as shown in Figure 3. The background absorption coefficient $\mu_a = 0.35\,\mathrm{mm}^{-1}$, the scattering coefficient $\mu_s = 23\,\mathrm{mm}^{-1}$, anisotropic parameter $g = 0.94$. In Figure 3(a), the background

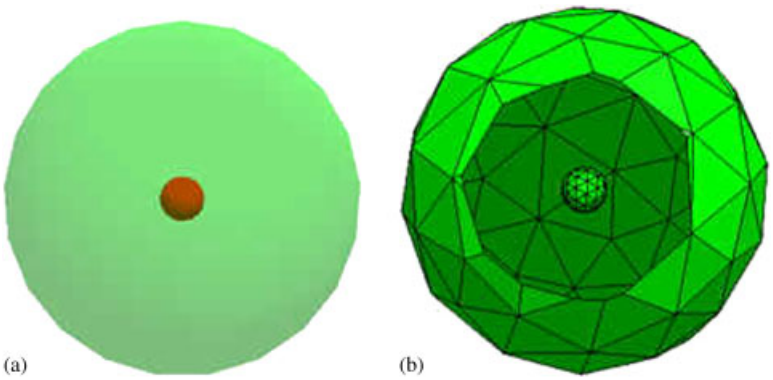

Figure 1. Homogeneous phantom: (a) lung tissue comprising a spherical source at its center and (b) the finite element mesh of homogeneous phantom.

DOI: 10.1002/cnm

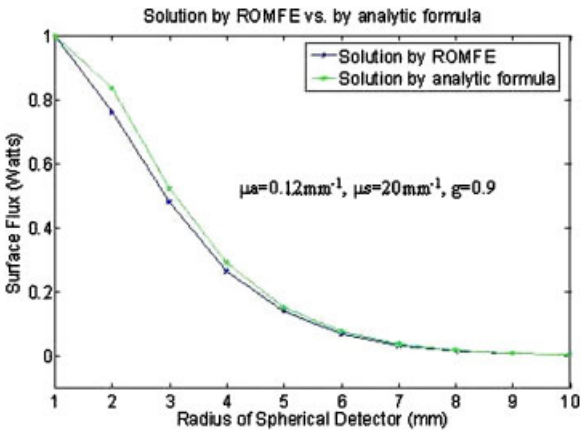

Figure 2. The comparison of forward solutions by ROMFE and by analytic formula.

Table I. ROMFE and analytic formula's comparison of surface flux and relevant errors.

Radius (mm)	ROMFE (W)	Analytic (W)	Error (%)
1	1	1	0.00
2	0.76	0.835	8.97
3	0.48	0.523	8.18
4	0.264	0.291	9.33
5	0.139	0.152	8.21
6	0.069	0.076	8.99
7	0.033	0.037	11.64
8	0.016	0.0177	8.97
9	0.0077	0.008	6.92
10	3.64E−03	3.84E−03	5.43

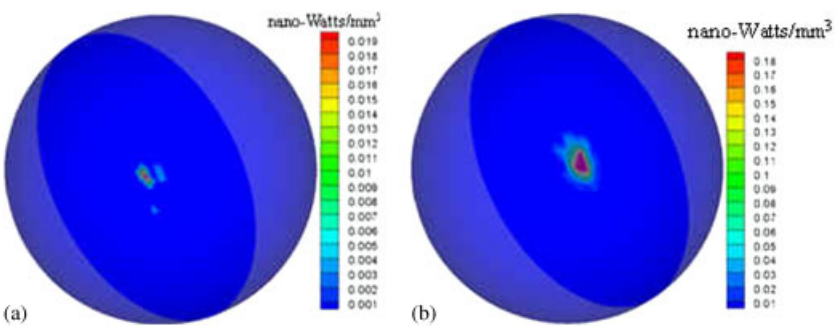

Figure 3. A comparison of ROMFE reconstruction of homogeneous phantom: (a) a cross section with coefficient errors and (b) a cross section with accurate coefficients.

DOI: 10.1002/cnm

optical coefficients have 50% errors and the maximal reconstruct density is $0.02\,\mathrm{nW/mm^3}$. While in Figure 3(b) with accurate optical coefficients, the maximal reconstruct density is $0.148\,\mathrm{nW/mm^3}$ that approximates the real density. The total reconstruction energy is near to the real total energy 1 W, which can approve the validation of ROMFE and the importance of background optical parameters as *a priori* information.

Table II lists the average source density, total power and position information of the reconstructed and real source. The average source density of ROMFE is $0.133\,\mathrm{nW/mm^3}$ and the total power error is about 10.986%. And the source position error is about 0.007 mm. From the comparison of reconstructed results and real source information, we can validate the proposed algorithm.

3.2. Heterogeneous experiment

In the second experiment, we utilize a heterogeneous phantom [19], which is a cylinder. It is 30 mm high with a radius of 10 mm. In the cylinder, there are four ellipsoids and one cylinder denotes left lung, right lung, heart, bone and liver, as illustrated in Figure 4(a). The bioluminescence spherical source is located at $(-3, 5, 15)$ in the right lung and the real total power is 1 nW.

MOSE (www.mosetm.net) is a forward model for bioluminescence light propagation based on statistical method. The intrinsic characteristic of MOSE is that Poisson noise is well integrated into the model that can depict the noise of surface flux.

In the forward simulation of MOSE, a spherical source with a radius of 1 mm and a power density of $0.238\,\mathrm{nW/mm^3}$ was utilized at the location of $(-3, 5, 15)$. The numbers of photons is 1.0×10^6. The forward mesh has 17 800 nodes and 86 123 tetrahedrons. On the other hand, the reconstruction initial mesh has 1537 nodes and 6878 tetrahedrons, which is completely different from the mesh used in MOSE. Thus, we can avoid the inverse crime effectively. The flux density on the boundary is computed by forward results generated by MOSE according to the principle of shortest distance. We let the domain $\{(x, y, z)|13<z<17, x<0, (x, y, z) \in \text{right lung}\}$ be the permissible source region. Optical parameters are listed in Table III.

We run two reconstruction simulations in contrast. One is the source reconstruction of ROMFE. The other is the source reconstruction of standard multigrid finite element (MFE) method [20]. MFE uses a series of mesh (from coarseness to fineness) to form a series of corresponding linear equation. By using the prolongation operator, MFE can transfer between the equations. After one mesh refinement on the possible source elements, the final reconstructed results of MFE and ROMFE are as shown in Figure 4(c) and (d).

These two simulations are executed on the same personal computer (Intel Pentium4, CPU 3.20 GHz, memory 1G). And the same initial mesh is used (mesh node: 1537 and mesh elements: 6878). The same MOSE forward solutions are matched. Before refinement, all conditions of these simulations are the same.

After one refinement, the number of mesh nodes of ROMFE is 1567 and that of elements is 7043, which can reduce the reconstruction dimension and raise the reconstruction stability in

Table II. The comparison of reconstructed results and real source in homogeneous phantom.

	Average density ($\mathrm{nW/mm^3}$)	Total power (W)	Source position (mm)
Real source	0.148	0.620	(0, 0, 0)
Reconstructed source	0.133	0.559	$(-0.0036, 0.0037, -0.0049)$

DOI: 10.1002/cnm

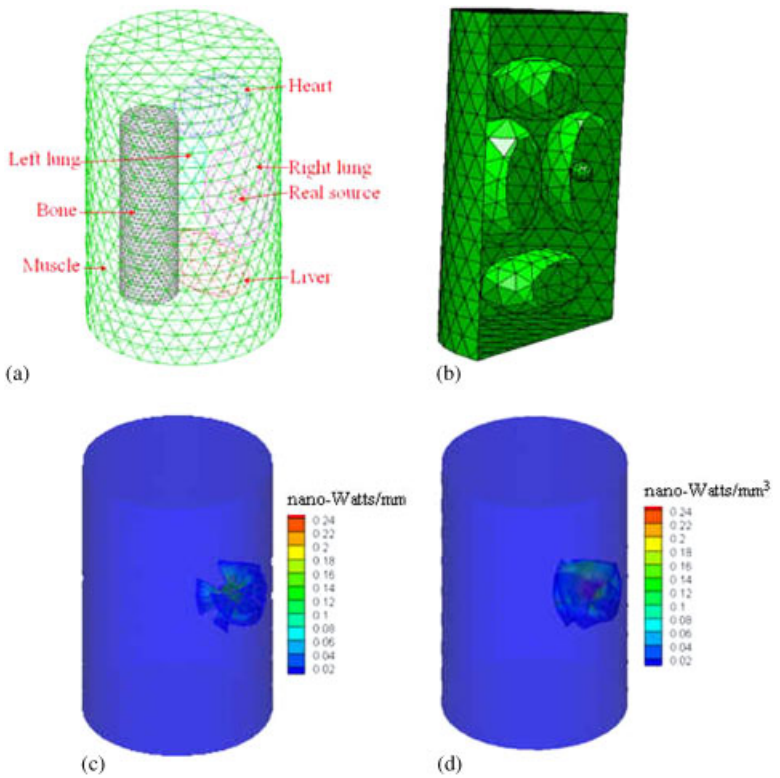

Figure 4. Heterogeneous phantom: (a) a real source in right lung; (b) the discretized mesh of ROMFE and MFE reconstruction; (c) reconstruction results of MFE; and (d) reconstruction results of ROMFE.

Table III. The optical parameters of the heterogeneous phantom.

Material	Muscle	Lung	Heart	Bone	Liver
$\mu_a(\text{mm}^{-1})$	0.01	0.35	0.2	0.002	0.035
$\mu_s(\text{mm}^{-1})$	4	23	16	20	6
g	0.9	0.94	0.85	0.9	0.9

comparison with MFE. The run time include the time of refinement, the matching of forward solution between MOSE and reconstruction algorithm, optimization algorithm, the generation of M^k_{mod} and F^k_{mod}, the inversion of $(M^k_{\text{mod}})^{-1}F^k_{\text{mod}}$ and display of three-dimensional image. The run time of ROMFE is 6 min, which is quicker than that of 20 min of MFE.

In Table IV,

$$\text{maximal density error} = \frac{|\text{real source density} - \text{maximal reconstruction density}|}{|\text{real source density}|}$$

DOI: 10.1002/cnm

Table IV. The comparison of reconstructed results of MFE and ROMFE in heterogeneous phantom.

	Maximal source density (nW/mm^3)	Average source density (nW/mm^3)	Total energy (W)	Finite mesh	Run time (min)
Real source	0.238	0.238	1		
MFE source	0.219	0.139	0.583	2156 nodes, 10 405 elements	20
ROMFE source	0.248	0.201	0.843	1567 nodes, 7043 elements	6

And the total energy error is defined in the same manner. We can see that the maximal source density of ROMFE is $0.248\,nW/mm^3$, which is near to the real source density and the maximal density error is 4.2%, which is better than that of MFE. The reconstructed total source power of ROMFE is $0.843\,nW/mm^3$ and the relevant error is 15.7%, which is also better than that of MFE. In contrast with MFE, we can get better reconstruction effects using ROMFE.

4. CONCLUSION

We have forwarded a novel reconstruction-oriented MFE algorithm, the feasibility and potential of which are demonstrated numerically. Taking source permissible region as *a priori* information can accurately reconstruct source distribution and density. Statistical method that generates forward data for reconstruction can avoid the inverse crime. Our future work is to validate the proposed algorithm using BLT system and real experiment.

ACKNOWLEDGEMENTS

This paper is supported by the Project for the National Key Basic Research and Development Program (973) under Grant No. 2006CB705700, Changjiang Scholars and Innovative Research Team in University (PCSIRT) under Grant No. IRT0645, CAS Hundred Talents Program, CAS Scientific Research Equipment Develop Program (YZ0642, YZ200766), 863 Program under Grant No. 2006AA04Z216, the Joint Research Fund for Overseas Chinese Young Scholars under Grant No. 30528027, the National Natural Science Foundation of China under Grant No. 30672690, 30600151, 30500131, 60532050, Beijing Natural Science Fund under Grant No. 4051002, 4071003.

REFERENCES

1. Contag C, Bachmann MH. Advances in bioluminescence imaging of gene expression. *Annual Review of Biomedical Engineering* 2002; **4**:235–260.
2. Wang G, Li Y, Jiang M. Uniqueness theorems in bioluminescence tomography. *Medical Physics* 2004; **31**: 2289–2299.
3. Klose AD, Ntziachristos V, Hielscher AH. The inverse source problem based on the radiative transfer equation in optical molecular imaging. *Journal of Computational Physics* 2005; **202**:323–345.
4. Ntziachristos V, Tung CH, Bremer C, Weissleder R. Fluorescence-mediated tomography resolves protease activity in vivo. *Nature Medicine* 2002; **8**(7):757–760.
5. Wang XD, Pang YJ, Ku G, Xie X, Stoica G, Wang LV. Noninvasive laser-induced photoacoustic tomography for structural and functional in vivo imaging of the brain. *Nature Biotechnology* 2003; **21**(7):803–806.

DOI: 10.1002/cnm

6. Cong W, Wang G, Kumar D, Liu Y, Jiang M, Wang LV, Hoffman EA, McLennan G, McCray PB, Zabner J, Cong A. Practical reconstruction method for bioluminescence tomography. *Optics Express* 2005; **13**(18):6756–6771.
7. Arridge SR, Schweiger M, Hiraoka M, Delpy DT. A finite element approach for modeling photon transport in tissue. *Medical Physics* 1993; **20**:299–309.
8. Chaudhari AJ, Darvas F, Bading JR, Moats RA, Conti PS, Smith DJ, Cherry SR, Leahy RM. Hyperspectral and multispectral bioluminescence optical tomography for small animal imaging. *Physics in Medicine and Biology* 2005; **50**:5421–5441.
9. Alexandrakis G, Rannou FR, Chatziioannou AF. Tomographic bioluminescence imaging by use of a combined optical-PET (OPET) system: a computer simulation feasibility study. *Physics in Medicine and Biology* 2005; **50**:4225–4241.
10. Dehghani H, Davis S, Jiang SD, Pogue B, Paulsen K, Patterson M. Spectrally resolved bioluminescence optical tomography. *Optics Letters* 2005; **31**:365–367.
11. Holder S. *Electrical Impedance Tomography*. Institute of Physics Publishing: Bristol, Philadelphia, 2005.
12. Li H, Tian J, Luo J, Lv Y, Cong WX, Hoffman EA, Wang G. Development of a molecular optical simulation environment. *Journal of Pattern Recognition and Artificial Intelligence* 2006.
13. Schweiger M, Arridge SR, Hiraoka M, Delpy DT. The finite element method for the propagation of light in scattering media: boundary and source conditions. *Medical Physics* 1995; **22**:1779–1792.
14. Rao SS. *The Finite Element Method in Engineering*. Butterworth-Heinemann: Boston, 1999.
15. Schwarz HR. *Finite Element Methods*. Academic Press: New York, 1988.
16. Kelley CT. *Iterative Methods for Optimization. Frontiers in Applied Mathematics*, vol. 18. SIAM: Philadelphia, 1999.
17. Bey J. Tetrahedral grid refinement. *Computing* 1995; **55**:355–378.
18. Cong WX, Wang LH, Wang G. Formulation of photon diffusion from spherical bioluminescent sources in an infinite homogeneous medium. *Biomedical Engineering Offline* 2004; **4**:12.
19. Lv Y, Tian J *et al.* A multilevel adaptive finite element algorithm for bioluminescence tomography. *Optics Express* 2006; **14**:8211–8223.
20. Hackbusch W. *Multi-Grid Methods and Applications*. Springer: Berlin, 1985.

DOI: 10.1002/cnm